Received: 26 November 2024 | Accepted: 7 May 2025

DOI: 10.1002/agj2.70089

Agronomy Journal

ORIGINAL ARTICLE

Biometry, Modeling, and Statistics

Low-input, interpretable models to forecast maize yield at multiple scales based on absorbed radiation

Martin Menendez-Coccoz[1] | **Diego H. Rotili**[1,2] | **María E. Otegui**[2,3] | **Gustavo Martini**[4] | **María Paolini**[4] | **Carlos Di Bella**[1] | **Gervasio Piñeiro**[1] | **Martín Oesterheld**[1]

[1]IFEVA, Universidad de Buenos Aires, CONICET, Facultad de Agronomía, Buenos Aires, Argentina

[2]Departamento de Producción Vegetal, Facultad de Agronomía, Universidad de Buenos Aires, Buenos Aires, Argentina

[3]Consejo Nacional de Investigaciones Científicas y Técnicas (CONICET) en INTA, Centro Regional Buenos Aires Norte, Estación Experimental INTA Pergamino, Pergamino, Argentina

[4]Unidad de Investigación y Desarrollo, Área de Agricultura, Asociación Argentina de Consorcios Regionales de Experimentación Agrícola (AACREA), Buenos Aires, Argentina

Correspondence
Martin Menendez-Coccoz and Martín Oesterheld, IFEVA, Universidad de Buenos Aires, CONICET, Facultad de Agronomía, Buenos Aires, Argentina.
Email: mamenendez@agro.uba.ar and oesterhe@agro.uba.ar.

Present Address
Martin Menendez-Coccoz, Kansas State University, Manhattan, KS 66506, USA.

Diego H. Rotili, América Agroinnova, América Buenos Aires, Argentina and Facultad de Agronomía, Universidad Nacional de La Pampa, Ruta Nacional 35, km 334, 6300 Santa Rosa, La Pampa, Argentina.

Assigned to Associate Editor QuanXiao Fang.

Funding information
Agencia Nacional de Promoción Científica y Tecnológica, Grant/Award Numbers: PICT2016-1258, PICT2020-02102

Abstract

Most crop yield forecast models operate at coarse scales (e.g., county or region) or need extensive input data for finer resolutions. Here, we present maize (*Zea mays* L.) yield forecast models that require minimal user data and operate at field and regional scales throughout the growing season. Using 1853 maize field-years in Argentina, with known location, sowing date, and yield, our models leveraged absorbed radiation (from satellite imagery), temperature-based phenology, regional site-year properties, El Niño-Southern Oscillation (ENSO) phase predictions, and sowing period. At the field scale, our models achieved high accuracy at physiological maturity, with a mean error of 1 t ha^{-1} (16%). Yield forecasts were mainly driven by absorbed radiation during the reproductive phase and a regional factor. Early-season forecasts incorporated ENSO and sowing period, but with reduced accuracy. When scaled to regional forecasts, the models performed even better, with a mean error of 0.3 t ha^{-1} (4%). These results combine a novel case of yield forecast because of the low data requirements from users, high anticipation (30–90 days before harvest), and good levels of accuracy at both field and regional scales. Additionally, the models' interpretability makes them valuable diagnostic tools for post-season analysis.

Plain Language Summary

Most crop yield forecasting models either work at large scales, like counties or regions, or need a lot of detailed input data to work at the field scale. In this study,

Abbreviations: APAR, absorbed photosynthetically active radiation; CP, critical period; ENSO, El Niño-Southern Oscillation; fAPAR, fraction of absorbed photosynthetically active radiation; HI, harvest index; MAE, mean absolute error; NDVI, normalized difference vegetation index; PARinc, incident photosynthetically active radiation; R6, physiological maturity; RUE, radiation use efficiency.

we developed simple models to forecast maize yields at both the field and regional scales, requiring minimal data from users. Our models use satellite data on sunlight absorbed by crops, temperature, and information about sowing dates and locations. We tested them with data from 1853 maize fields in Argentina. At the field scale, the models had an average error of 1 t/ha (16%), and at the regional scale, they performed even better, with an error of just 0.3 t/ha (4%). The most important factor for accurate forecasts was sunlight absorbed during the reproductive phase of the crop. These models allow farmers and researchers to forecast yields earlier before harvest and understand what influences crop performance, supporting better agricultural decisions.

1 | INTRODUCTION

Forecasting crop yield is important for logistical, social, scientific, and financial purposes (Benami et al., 2021; Burke et al., 2020; Lobell, 2013). Early yield forecasts allow various stakeholders in the crop production and commercialization chain to make informed decisions (Paudel et al., 2022; van der Velde et al., 2019). For instance, at the field scale, farmers can organize harvest and storage logistics, take positions in the futures market, or determine optimal management practices. Additionally, these field-scale forecasts can be scaled up to support regional crop monitoring systems, enabling governments or NGOs to anticipate production and design better strategies to ensure food security (Deines et al., 2021). Maize (*Zea mays* L.), in particular, is grown worldwide and valued as food for human or animal consumption, and more recently, for its use in biofuel production (FAO, 2023). For this reason, having an accurate forecasting system for maize yield that requires minimal data to operate and is applicable at both field and regional scales is highly important.

Different approaches have been suggested to forecast crop yield at different scales (Basso & Liu, 2019). At the regional level, regression models between yield and climate variables, such as temperature or precipitation, were used very early on (Murata, 1975; Thompson, 1969). At the field or sub-field level, crop simulation models forecast yield based on several input variables such as genotype, weather conditions, and management practices (Chipanshi et al., 1997; Hodges et al., 1987). However, they need extensive input data, which limits their practical application. In contrast, models based on remote sensors that provide information on radiation absorption require less input data to operate effectively at the field scale (Peralta et al., 2016; Schwalbert et al., 2018).

Combining these approaches has been the basis for developing operating systems that monitor crop status in real time and forecast yield (Basso & Liu, 2019; Fritz et al., 2019; Huang et al., 2019; Johnson, 2014). Schauberger et al. (2020) summarized key features of the state of the art in crop yield forecasts. They concluded that most of the research (1) focuses on wheat (*Triticum aestivum*), maize, and rice (*Oryza sativa*); (2) is carried out in the United States and China; (3) forecasts at coarser scales, such as the county or national scales, with only 17% at the field scale; (4) achieved R^2 between 0.6 and 0.8, with few studies reporting other accuracy metrics; and (5) lacks validation of their results with independent data not used for calibration.

To achieve accurate and efficient yield forecasts from field to regional scales, it is crucial to develop models that require minimum input data from users. Additionally, it is also desirable that the models are informative and interpretable. A convenient framework for achieving this type of model is the crop growth and yield analysis based on the absorption of solar radiation and its conversion efficiency into biomass and yield ("Monteith model," Monteith, 1972; Monteith, 1994). Thus, yield can be represented as the product of the accumulation of incident photosynthetically active radiation (PARinc) during the crop cycle, the fraction of it that is absorbed (fraction of absorbed photosynthetically active radiation [fAPAR]), the radiation use efficiency (RUE), which represents the conversion of absorbed radiation into aboveground biomass, and the harvest index (HI), which quantifies the yield per unit of aboveground biomass (Equation 1):

$$\text{Yield} = \text{PARinc} \times \text{fAPAR} \times \text{RUE} \times \text{HI} \quad (1)$$

This model has been used to explain crop yield variation in terms of absorbed radiation inferred from remote sensing data (e.g., normalized difference vegetation index [NDVI], GCVI, Gitelson et al., 2014; Pellegrini et al., 2020) and conversion efficiency derived from empirical modeling (Andrade et al., 2022; Rattalino Edreira et al., 2020).

Combining the "Monteith model" with the use of remote information derived from satellite images has several advantages. The fine spatial and temporal resolution of current satellites enables crop data collection at the field or sub-field scale, which may be used to train models that forecast yield during the crop cycle without requiring additional data. In turn, the "Monteith model" establishes a common language

among users, including those unfamiliar with remote sensing concepts, so that yield variations are explained in terms of their eco-physiological components (PARinc, fAPAR, RUE, and HI), and the model may be used to diagnose field performance. Combining satellite information with Monteith's approach provides more information than simple correlations between yield and vegetation indices, requires low-input data from users, and can work at different spatial and temporal scales.

The objectives of this study were to (1) develop field-scale models to forecast maize yield using absorbed radiation up to physiological maturity (R6); (2) develop field-scale models to forecast yield at different stages of the crop cycle; and (3) scale up the results from the previous objectives to forecast yield at the regional scale throughout the growing season.

Core Ideas

- Low-data input models to forecast maize yield at field and regional scales.
- Models incorporate phenology-adjusted absorbed radiation and production regions.
- Field-scale forecasts had a mean error of 1 t ha^{-1} (16%).
- Regional-scale forecasts had a mean error of 0.3 t ha^{-1} (4%).
- Interpretable models explain yield variations across fields, years, and regions.

2 | MATERIALS AND METHODS

2.1 | General description of the methodology

The methodology of this study consisted of six steps:

1. We compiled a database with yield, sowing date, and latitude-longitude of 1853 maize fields across four years (2017–2021) and eleven regions that encompass nearly the entire maize-growing area of Argentina (Figure 1A,B).
2. For each field-year, we extracted time series of temperature, PARinc, and NDVI (Figure 2).
3. We estimated absorbed radiation during the entire crop cycle and particular phenological stages from NDVI and PARinc (Figure 2).
4. To achieve the first objective, we calibrated and validated regression models that forecasted the yield of each field-year from absorbed radiation up to R6. Additionally, we evaluated whether the models differed by region, El Niño-Southern Oscillation (ENSO) phase, or sowing period.
5. For the second objective, we calibrated and validated regression models using the information on absorbed radiation at different time intervals from the sowing date.
6. For the third objective, we assessed forecasted yield at a regional scale throughout the crop season, as fields were sown and progressed throughout their cycle.

2.2 | Study area

The study area extends from 26° S to 39° S and from 57° W to 66° W (Figure 1A). It covers approximately 90% of the Argentinean maize production area (ReTAA, 2022). Environmental conditions and maize management practices vary widely across the area (Maddonni, 2012; Satorre & Andrade, 2022). The frost-free period decreases from 180 days in the north to 140 days in the south. Similarly, the average annual temperature decreases from 21.5°C to 15.7°C. Precipitation decreases from east to west, from approximately 1000 to 600 mm per year. Maize is grown in extensive fields. In our database, the median sowed area of a single field within a farm was 72 ha, with a minimum of 8 ha and a maximum of 700 ha. A >95% of the sowing area is under the "no-till" system. Sowing density varies from 3 plant m^{-2} in yield-limiting environments to 11 plant m^{-2} in high-production environments. The sowing dates are divided between early and late sowings. Since most of the maize crops in Argentina are rainfed, the main difference between early and late sowings is the development of the cycle in relation to water balance. In the central region of Argentina (32–38 °S), early-sown maize is sown in September–October, and its critical period (CP) (Cerrudo et al., 2013) occurs during late December and the first days of January (Cirilo & Andrade, 1994; Otegui et al., 1995). Late-sown maize, on the other hand, is sown in December–January, and its CP occurs along February and March (Mercau & Otegui, 2014). Therefore, early sowing is carried out where favorable water conditions are expected in January, while late sowing is carried out where unfavorable water conditions are expected in January (Otegui et al., 2021). Maize grown in the northern region (latitude <32°S) is almost totally sown in December–January to avoid the risk of heat shock during the CP (Otegui et al., 2023).

We partitioned the area into eleven regions defined by the CREA movement (Figure 1A,B). The CREA movement brings together >2000 farming companies that meet monthly in regional groups to share experiences and information, while also generating technology and knowledge for the sustainable development of companies (https://www.crea.org.ar/mision-y-vision/). Thus, farming companies within each region share not only information about edaphoclimatic conditions but also the guidelines for crop management.

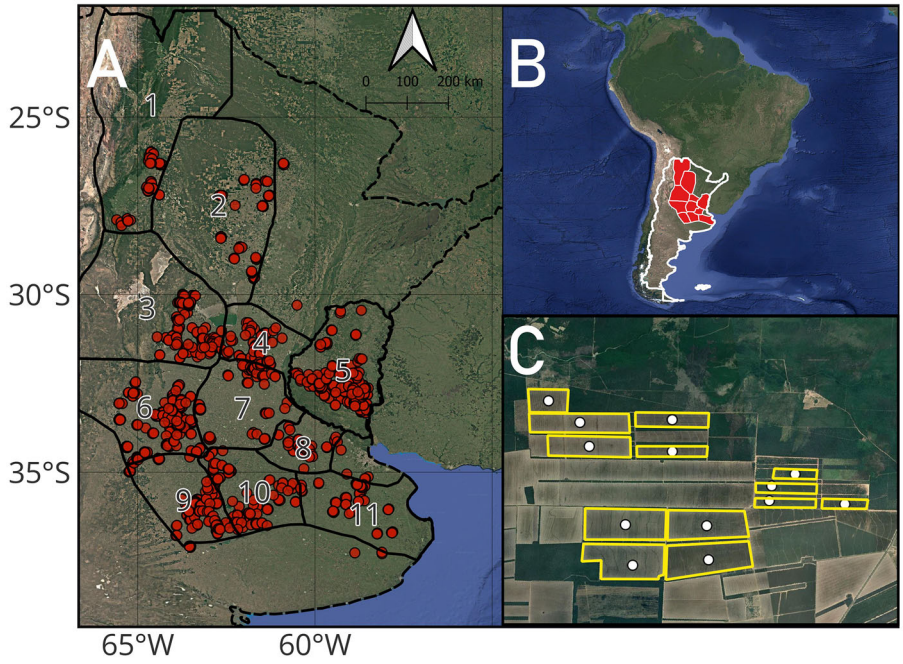

FIGURE 1 Study area and example of delimitation of production field boundaries. (A) Study area. The red dots refer to the 1853 field observations during the four seasons, solid black lines with numbers refer to the eleven regions, and dashed black lines refer to Argentina's national boundaries. Fields outside regions were assigned to the nearest one. (B) Location in South America and production regions as classified by CREA. (C) Delimitation of fields. The white dots refer to the geographic coordinates reported by the farmer, and the yellow polygons refer to the boundaries of the fields delimited by photointerpretation.

2.3 | Agronomic database

We compiled a field-scale database from the agricultural traceability database of CREA (DAT CREA, https://crea.org.ar/). To be included, maize fields had to be destined to grain production and have geographic coordinates. These fields were sown with maize in at least one of four growing seasons: 2017–2018, 2018–2019, 2019–2020, and 2020–2021. Initially, the dataset comprised 3031 unique field-year observations that included information on year, field, sown area, sowing date, and yield as reported by farmers (typically at 14% moisture).

Using geographic processing, we delimited a polygon of the field boundaries around each geographic coordinate by visually inspecting "Sentinel-2" satellite images from January–February of each growing season. We verified that the area of the drawn polygon matched the area reported in the database (Figure 1C, QGIS Development Team, 2022). As a result, we discarded 449 records because of incorrect geographic coordinates or fuzzy boundaries.

2.4 | Climate and vegetation index databases

We compiled a second database with daily PARinc and mean temperature for each field-year. For PARinc, we obtained monthly averages from the Instituto Nacional de Pesquisas Espaciais (INPE). INPE reports monthly average PARinc with a spatial resolution of 4 km (Martins et al., 2017). We assumed each monthly record to correspond to the 15th of the month and estimated daily data by linear interpolation between subsequent records. For daily mean temperature, we obtained the data from the Prediction of Worldwide Energy Resource (NASA POWER, https://power.larc.nasa.gov/data-access-viewer/), which reports this variable with an approximate spatial resolution of 60 km.

We compiled a third database with daily NDVI for each field-year during the crop cycle. We used the "MODIS NDVI 16-Day 250 m" product on board the "TERRA" satellite (MOD13Q1, Didan et al., 2015). The product has a spatial resolution of ~250 m and provides the maximum NDVI value every 16-day period, which we assigned to the day of year (DOY) reported by the product as the representative date for that period. Data were extracted from pixels that presented at least 90% of their area within the field polygon. We obtained daily data by linear interpolation. We discarded 724 field-year combinations because they either had data gaps longer than 40 days (due to low-quality informed from the product) or were not covered by at least one pixel (Irisarri et al., 2018). The median number of pixels per field-year was 6 (~37.5 ha), with a minimum of 1 and a maximum of 110 pixels. The median number of NDVI observations per field-year was 9, with a minimum of 6 and a maximum of 11.

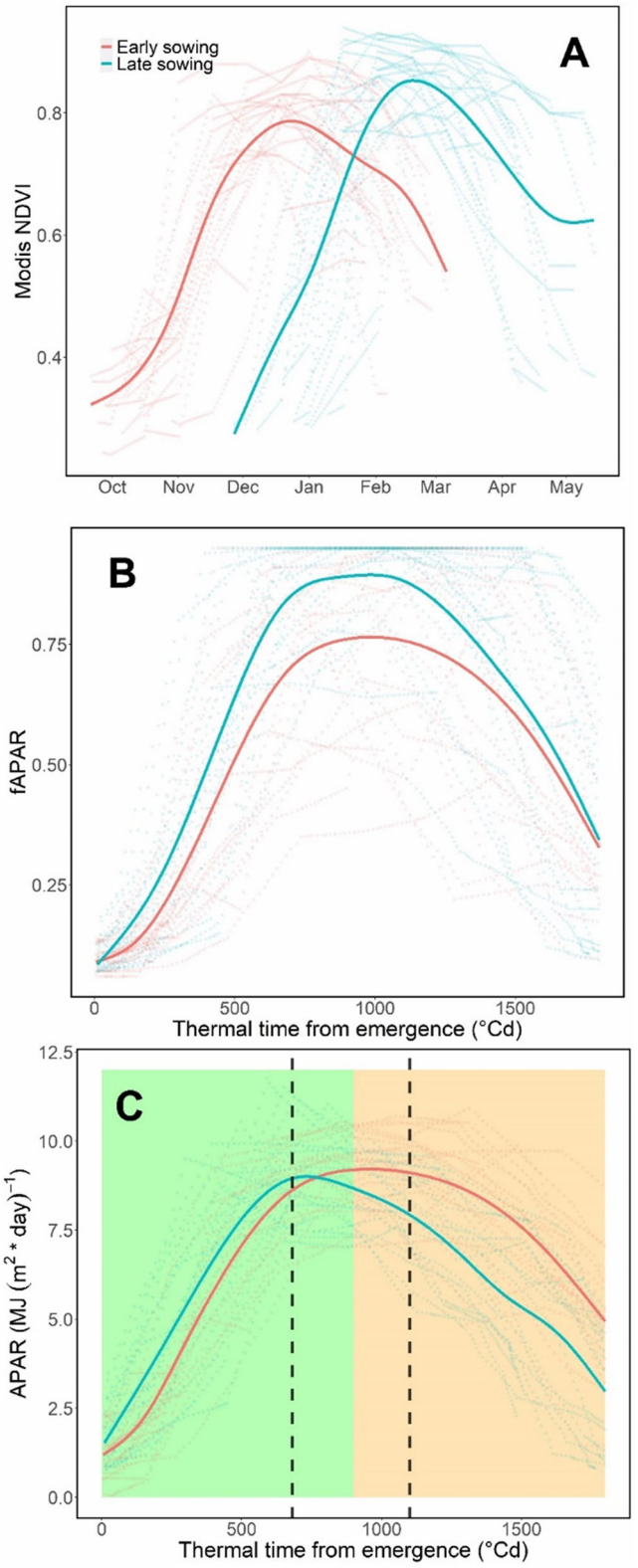

FIGURE 2 Method for estimating the absorbed radiation (absorbed photosynthetically active radiation [APAR]) for each field-year based on normalized difference vegetation index (NDVI) and its conversion to fraction of absorbed photosynthetically active radiation (fAPAR) and APAR. Just for illustration purpose, we show 20 random fields from the 2020-2021 crop season (dotted lines) for early and late sowings. Solid lines represent their smoothed fit. (A) Time series of NDVI from the MODIS sensor. (B) fAPAR as a function of crop thermal time from emergence. fAPAR was derived from the model by Gitelson et al. (2014), and thermal time was derived from the model by Maddonni (2012). (C) Daily APAR, the product of fAPAR and incident PAR, as a function of thermal time. The shaded green area corresponds to the vegetative phase (0°C–900°C day), the shaded orange area corresponds to the reproductive phase (900°C–1800°C day), and the area delimited by black dotted lines corresponds to the critical period (680°C–1100°C day).

(Continues)

TABLE 1 Phenological phases and their thermal time and base temperature as considered in Maddonni (2012).

Phenological phase	Thermal time (°C day)	Base temperature (°C)
S–VE	90	10
VE–R1	900	8
R1–R6	900	8

Note: S–VE: Sowing–emergence. VE–R1: Emergence-silking. R1–R6: Silking–physiological maturity.

2.5 | Estimation of crop cycle, phenological stages, and absorbed radiation

We considered the following phenological phases for each field-year (Ritchie & Hanway, 1982): sowing (S)—emergence (VE), VE—female flowering or silking (R1), and R1—physiological maturity (R6). In addition, we assigned the CP as 220° days before and 200° days after R1 with a base temperature of 8°C (Cerrudo et al., 2013; Otegui & Bonhomme, 1998). The sowing date was obtained from the agronomic database, while the rest of the phases were estimated using a thermal time accumulation model based on temperature data from the climate database (Maddonni, 2012; Table 1). The whole crop cycle for each field year was considered as the period between VE and R6. For those field-years that experienced a daily average temperature lower than 8°C during the final reproductive phase, the crop cycle was interrupted because early frosts at this stage stop effective grain filling. Similarly, for those field-years that had not reached R6 by June 1, the crop cycle was interrupted due to the possibility of frost damage.

For each field-year, we calculated the absorbed radiation (absorbed photosynthetically active radiation [APAR]) during the entire crop cycle (VE–R6, VE–R1, and R1–R6) and the CP in three calculations (Figure 2). First, we transformed NDVI to the fAPAR. This was done using empirical models between field-measured fAPAR by maize and MODIS NDVI (Gitelson et al., 2014). For the VE–R1 phase, the model was fAPAR = 1.35 NDVI–0.32 ($R^2 = 0.95$), while for the R1–R6 phase, the model was fAPAR = 1.89 NDVI – 0.78 ($R^2 = 0.93$).

TABLE 2 Variation of relevant components of Monteith's model (Equation 1) in the database: Total incident radiation (incident photosynthetically active radiation [PARinc]), average absorption efficiency (fraction of absorbed photosynthetically active radiation [fAPAR]), total absorbed radiation (APAR), yield, and grain conversion efficiency.

Parameter	PARinc (MJ m^{-2})	Average fAPAR	APAR (MJ m^{-2})	Yield (t ha^{-1})	Grain conversion efficiency (g MJ^{-1})
Minimum	790	0.11	150	3.4	0.05
Percentile 25	1312	0.49	704	6.22	0.84
Mean	1439	0.55	784	8.00	1.01
Median	1495	0.54	797	8.16	1.03
Percentile 75	1575	0.61	873	9.96	1.19
Maximum	1931	0.78	1177	15.30	1.79

When necessary, negative fAPAR values were set to 0, while values >0.95 were set to 0.95. Second, we calculated daily APAR as the product of daily fAPAR and PARinc. Finally, we calculated APAR during the entire cycle or phenological phase as the sum of the corresponding daily APAR values between the corresponding thermal time thresholds.

We eliminated five records with likely erroneous data because of their high grain conversion efficiency, defined as the ratio of yield to accumulated APAR. The grain conversion efficiency is equal to the product of RUE and HI. According to the literature, the maximum value of RUE for a maize crop is 3.8 g MJ^{-1} (Lindquist et al., 2005), while the maximum HI is approximately 0.5 (Echarte & Andrade, 2003). Their product results in a maximum grain conversion efficiency of 1.9 g MJ^{-1}. The five records exceeding this threshold were discarded due to their high probability of being erroneous.

2.6 | Data analysis

The final database consisted of 1853 unique field-year observations that showed a large variation of Monteith's model components (Table 2). In relative terms, the highest variation among field-years was observed in yield, which varied by 60% between the 25–75 percentiles. This was followed by conversion efficiency (42%), total APAR and average fAPAR throughout the cycle (both 24%), and finally PARinc (20%). For additional details on the number of field-year observations and average yield across regions, years, and sowing periods, see Table S1.

We incorporated APAR during the different phenological phases as continuous variables, and production region, ENSO phase, and sowing period as categorical variables. APAR during each phase was incorporated both as its raw and quadratic value. The production region variable was based on the grouping shown in Figure 1A. The ENSO phase was analyzed by classifying the growing seasons into two categories based on the December–January–February quarter: "La Niña" (seasons 2017–2018 and 2020–2021) and "Not La Niña" (seasons 2018–2019, which corresponded to "El Niño," and 2019–2020, which was Neutral). This classification was based on monthly ENSO forecasts provided by the International Research Institute for Climate and Society (https://iri.columbia.edu/). In the central part of our study area, "La Niña" phases are associated with reduced rainfall during late spring and early summer, leading to lower maize yields (Podestá et al., 1999). The sowing period was included as a categorical variable with two levels: "Early" or "Late." The classification was based on the sowing date relative to December 1 in regions located north of latitude 32° S and relative to November 20 in regions located further south. Finally, the interaction between ENSO phase and sowing period was analyzed by grouping these two variables into four categories: "Early—La Niña," "Early—Not La Niña," "Late—La Niña," and "Late—Not La Niña."

To achieve the first objective (field-scale models that forecast yield from APAR up to R6), we calibrated and validated simple and multiple regression models between yield and APAR during the entire crop cycle (VE–R6), VE–R1, R1–R6, and the CP. We also explored whether the productive region, the ENSO phase, or the sowing period (early- vs. late-sown) increased the predictive power. In this way, we obtained models that predicted yield with all the available information at the end of the crop cycle, 30 (early sowings) to 90 days (late sowings) before harvest.

To achieve the second objective (field-scale models that forecast yield at different stages of the crop cycle), we calibrated and validated models that predicted the yield of each field from its sowing date onward. These models were calibrated with information from 40 to 140 days after sowing at regular intervals of 20 days. The 20-day interval is approximate, as it was obtained by cutting every 20 days the interpolated daily series of the MODIS product, whose original temporal resolution was 16 days. This procedure resulted in a "library of models" that best predicted yield given the information available up to a certain moment in the crop cycle.

To achieve the third objective (forecast maize yield at a regional scale throughout the crop season), we predicted the yield of each field on the 15th day of each month throughout the growing season (November—June). Model selection

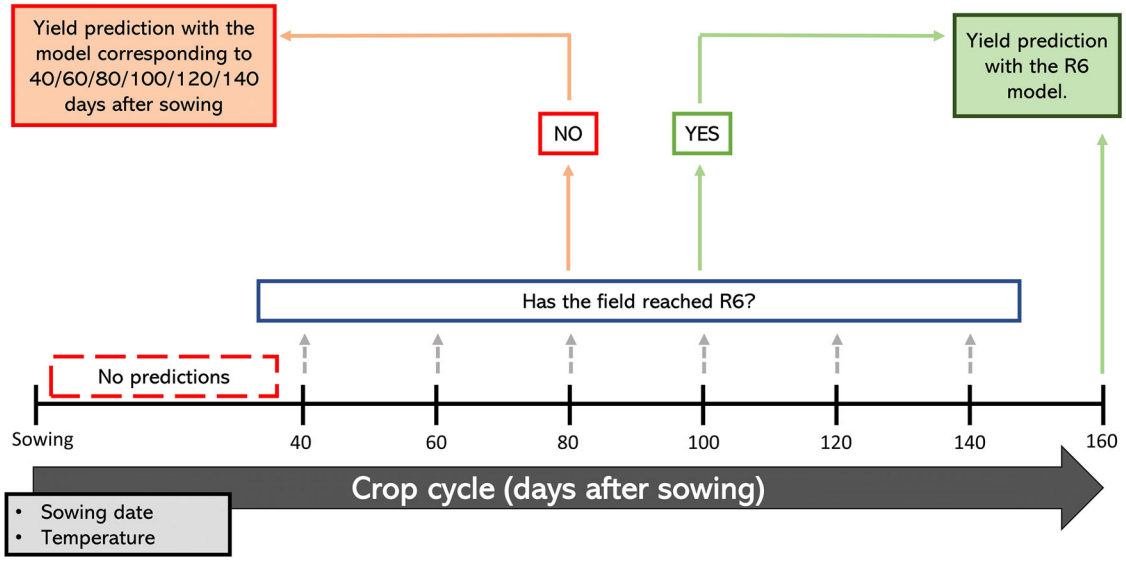

FIGURE 3 Use of the library of models to predict yield of a given field. From 40 days after sowing, yield was predicted by the corresponding model, unless the field had reached R6, in which case it was predicted by the R6 model developed for objective 1.

followed the pattern described in Figure 3: at any given date, we first checked if the field had reached R6, in which case it was assigned the model validated for objective 1. Otherwise, we assigned the best model of the library of models given the time after its sowing date. The predictions for individual fields were averaged by region, year, and sowing period. The regional yield prediction was compared with the observed regional yield for each calendar date and sowing period. For this regional-level analysis, we included the 35 combinations of region—year—sowing period with at least 15 data point (fields; see Table S1 for more details on the combinations included).

For model development, we used the 5-fold cross-validation method. This method involves randomly dividing the dataset into five equal parts, using four for model calibration and the fifth for validation, and repeating this process until the model has been validated across all parts. To obtain parsimonious models, we applied the following selection criterion: First, we calculated the mean absolute percentage error (MAPE, %) of a null model, which makes predictions using only the mean yield from the calibration dataset. Then, we calibrated all possible models with a single predictor variable and selected the one with the lowest validation MAPE, provided that it reduced the null-model MAPE by at least 1%. If this condition was met, we compared the new model with the best model, including two predictor variables, provided that the second variable further reduced the previous model MAPE by at least 1%. This process was repeated until adding one more predictor variable resulted in a reduction of <1% in the validation MAPE.

In addition to MAPE, we reported model accuracy with mean absolute error (MAE) and adjusted R^2 as validation metrics (Equations 2–4):

$$\text{MAPE}\ (\%) = \frac{1}{n}\sum_{i=1}^{n}\left|\frac{\text{Observed yield} - \text{Predicted yield}}{\text{Observed yield}}\right| \times 100 \quad (2)$$

$$\text{MAE}\ \left(\text{t ha}^{-1}\right) = \frac{1}{n}\sum_{i=1}^{n}\left|\text{Observed yield} - \text{Predicted yield}\right| \quad (3)$$

$$R^2_{\text{adj}} = \left(\frac{\left(1 - R^2\right) \times (n-1)}{n-k-1}\right) \quad (4)$$

where n is the total number of observations, k is the number of predictor variables, and R^2 is the standard coefficient of determination.

All analyses were performed using the statistical software "R" and the "caret" and "tidyverse" packages (Kuhn, 2008; R Core Team, 2021; Wickham et al., 2019).

3 | RESULTS

3.1 | Field-scale yield forecasts at physiological maturity

Based solely on APAR, the spatial and temporal variation of maize yield in Argentina was best predicted at R6 by the radiation absorbed during the reproductive phase (R1–R6, $R^2_{\text{adj}} = 0.59$, MAE = 1.3 t ha^{-1}, MAPE = 21%, Figure 4A). This period had greater predictive power than either the vegetative phase (VE—R1, $R^2_{\text{adj}} = 0.11$, MAE = 2 t ha^{-1}, MAPE = 35%) or the CP ($R^2_{\text{adj}} = 0.30$, MAE = 1.79 t ha^{-1},

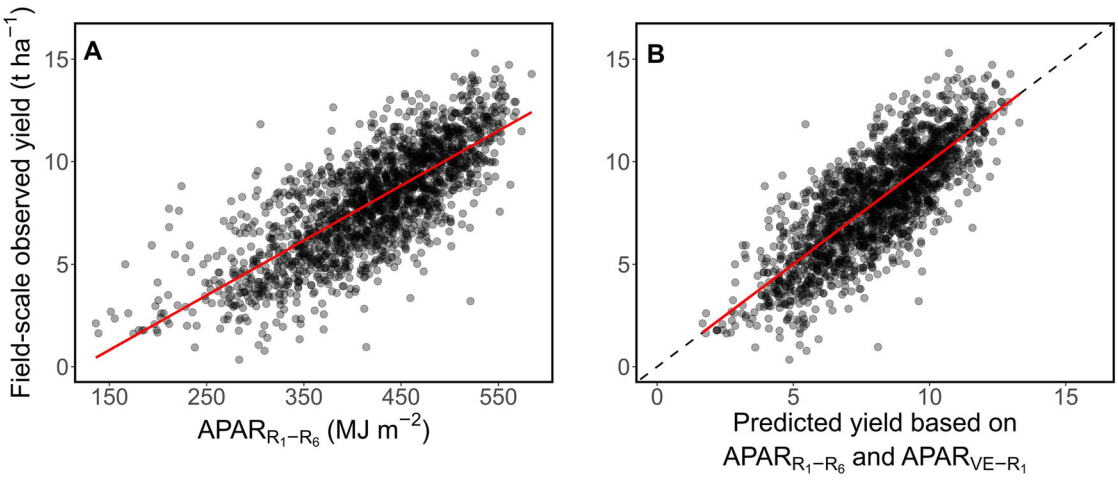

FIGURE 4 Validation of models that predicted yield based on absorbed radiation (absorbed photosynthetically active radiation [APAR]) up to R6. Each dot is an observation of a field year. (A) Field-scale observed yield as a function of APAR during the reproductive phase. The red solid line represents the prediction of the model. Yield = −3.22 + 0.027 $APAR_{R1–R6}$. (B) Observed yield as a function of predicted yield by the model Yield = 0.17 + 0.000032 $APAR_{R1–R6^{\wedge}2}$ + 0.0057 $APAR_{VE–R1}$, which considers radiation absorbed during the reproductive (quadratic value) and vegetative phases. The dotted black line represents the line $y = x$. The red solid line represents the fit between observed and predicted yield.

MAPE = 30%). Combining the APAR during the vegetative and reproductive phases into a multiple regression model had greater predictive power than each phase individually (R^2_{adj} = 0.63, MAE = 1.26 t ha^{-1}, MAPE = 20%, Figure 4B) or the entire cycle (VE—R6, R^2_{adj} = 0.47, MAE = 1.5 t ha^{-1}, MAPE = 25%). In other words, distinguishing the phenological phase in which radiation was absorbed significantly increased the predictive power of the model compared to considering the APAR throughout the entire cycle (R^2_{adj} = 0.63 vs 0.47). This multiple regression model incorporated the effect of the APAR during the reproductive phase with its quadratic term.

The predictive power of the model notably increased by including the production region as a categorical variable (R^2_{adj} = 0.72, MAE = 1.06 t ha^{-1}, MAPE = 18%), whereas it was just marginally increased by including the ENSO phase or the sowing period (early vs. late). The models for each region had a slightly higher predictive power thanks to the inclusion of phenological phases or ENSO in some regions (R^2_{adj} = 0.74, MAE = 1.03 t ha^{-1}, MAPE = 16%, Figure 5). The fit and residuals varied among the production regions (Figures 5 and 6). For example, R^2_{adj} ranged from 0.4 to 0.88, MAE from 0.79 to 1.35 t ha^{-1}, and MAPE from 11.2% to 26.8%. In relative terms, 10 out of eleven regions exhibited good error metrics, with MAPE below 20%, whereas models were not accurate for region 11, which had a MAPE of 26.8%.

Ten out of the eleven regions included the APAR during the reproductive phase (Table 3), whereas one incorporated only the radiation absorbed during the entire cycle (region 11). In turn, two regions incorporated the effect of APAR during the CP (regions 1 and 6). Regarding categorical variables, only one region incorporated the effect of the interaction between ENSO phase and sowing period (region 6). In some regions, the sowing period was not a candidate variable because they grew either exclusively early (e.g., region 5) or late maize crops (e.g., regions 1 and 2).

3.2 | Field-scale yield forecasts at different stages of the crop cycle

As the crop cycle progressed from emergence to R6, more information about APAR was incorporated, and yield was predicted more accurately (Figures 7 and 8; Table S2). Globally, from 40 days after sowing to R6, R^2_{adj} increased from 0.37 to 0.74, MAE decreased from 1.62 to 1 t ha^{-1}, and MAPE from 29% to 16%. Again, fit and errors depended on the region. The increase in R^2_{adj} and decrease in MAE and MAPE were larger in some regions (e.g., regions 2 and 6) than others (e.g., regions 1 and 5). The latter was due to low final adjustment (e.g., region 1) or high accuracy of early-cycle predictions (e.g., region 5).

The variables included in the models changed as the crop progressed (Figure 9). The earliest models mainly considered the ENSO phase or the sowing period, and only a few incorporated APAR variables. In fact, for regions 1 and 7, predicting yield using only the mean was the best-performing model (see null R^2_{adj} values in Figure 7). As the crop cycle progressed, more satellite images became available for each field, providing additional information that increased the importance of APAR in the models. In the early models, APAR during the elapsed period was the most important variable. Later, when it was possible to differentiate APAR during the reproductive phase, this variable gained participation in the models.

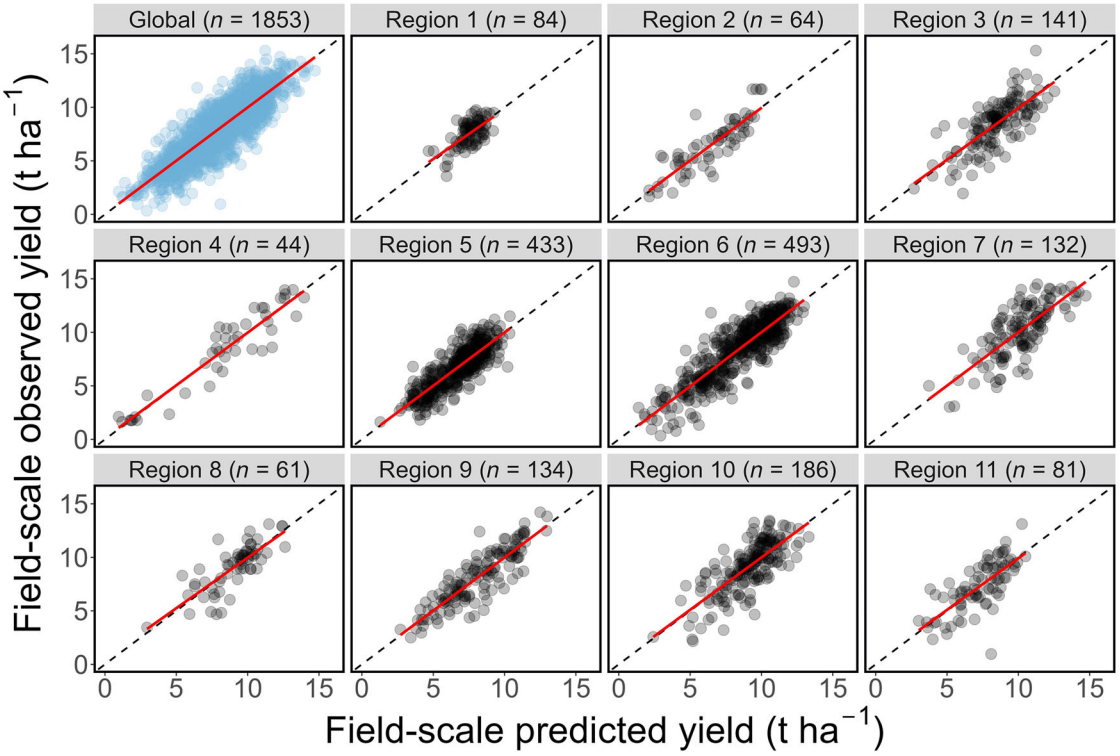

FIGURE 5 Observed yield as a function of predicted yield for the global database (top left panel, blue dots) and each region. Each dot represents a field year. The black dotted line represents the $y = x$ line. The red solid line represents the fit between observed and predicted yield. Predicted values were obtained from the models for each region (Table 3). For the location of the regions, see Figure 1A.

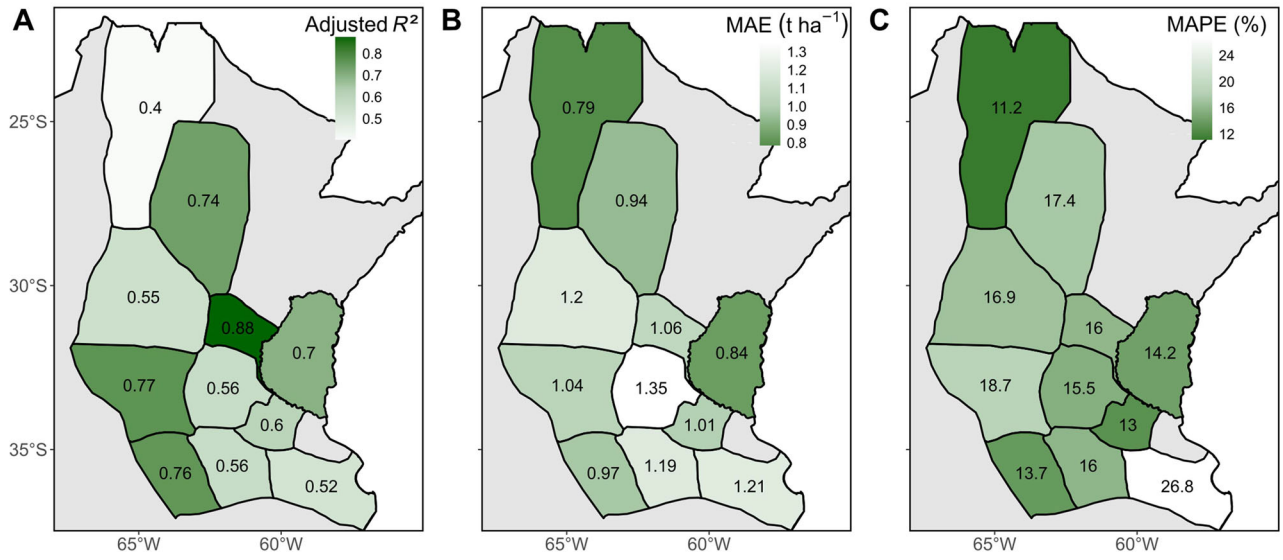

FIGURE 6 Performance by region of field-scale models with information up to R6. (A) Validation R^2_{adj} of the models for each region as in Table 3. (B) mean absolute error (MAE) for each region. (C) Mean absolute percentage error (MAPE) for each region.

APAR during the CP of the crop was important for models between 80 and 120 days after sowing, probably because flowering occurs around that time window. Subsequently, its contribution to the models decreased, probably because it was encompassed by APAR during the reproductive phase.

TABLE 3 Models for forecasting maize yield using all available information up to R6 for each region. Yield: kg ha^{-1}, absorbed photosynthetically active radiation (APAR) (absorbed radiation): MJ m^{-2}.

Region	Formula
Region 1	$\text{Yield} = -795 + 0.019 \times \text{APAR}_{\text{R1–R6}^{\wedge}2} + 30.9555 \times \text{APAR}_{\text{CP}}$
Region 2	$\text{Yield} = -5605 + 29.0735 \times \text{APAR}_{\text{R1–R6}} + 8.538 \times \text{APAR}_{\text{VE–R1}}$
Region 3	$\text{Yield} = -4540 + 27.373 \times \text{APAR}_{\text{R1–R6}} + 0.0164 \times \text{APAR}_{\text{VE–R1}^{\wedge}2}$
Region 4	$\text{Yield} = -977 + 0.0401 \times \text{APAR}_{\text{R1–R6}^{\wedge}2} + 8.9592 \times \text{APAR}_{\text{VE–R1}}$
Region 5	$\text{Yield} = -1652 + 11.5195 \times \text{APAR}_{\text{R1–R6}} + 0.0058 \times \text{APAR}_{\text{VE–R6}^{\wedge}2}$
Region 6	$\text{Yield} = -5447 + 24.0066 \times \text{APAR}_{\text{R1–R6}} + 0.0538 \times \text{APAR}_{\text{CP}^{\wedge}2} - 209 \times$ "ES-Niña" $- 122 \times$ "LS-Niña" $- 988 \times$ "LS-Not Niña"
Region 7	$\text{Yield} = -1066 + 0.0318 \times \text{APAR}_{\text{R1–R6}^{\wedge}2} + 12.2376 \times \text{APAR}_{\text{VE–R1}}$
Region 8	$\text{Yield} = -2522 + 18.8998 \times \text{APAR}_{\text{R1–R6}} + 0.0042 \times \text{APAR}_{\text{VE–R6}^{\wedge}2}$
Region 9	$\text{Yield} = 1003 + 0.0291 \times \text{APAR}_{\text{R1–R6}^{\wedge}2} + 0.0107 \times \text{APAR}_{\text{VE–R1}^{\wedge}2}$
Region 10	$\text{Yield} = -6314 + 22.7792 \times \text{APAR}_{\text{R1–R6}} + 11.902 \times \text{APAR}_{\text{VE–R1}}$
Region 11	$\text{Yield} = -5829 + 16.3803 \times \text{APAR}_{\text{VE–R6}}$

Note: R1–R6: reproductive phase (silking—physiological maturity). VE—R1: vegetative phase (emergence—silking). VE—R6: complete crop cycle (emergence—physiological maturity). CP: critical period. The symbol "$_{\wedge}2$" means that the variable was incorporated with its quadratic value. "ES-Niña": Early sowing and La Niña ENSO phase. "LS-Niña": Late sowing and La Niña ENSO phase. "ES-Not Niña": Early sowing and Not La Niña ENSO phase. The model for region 6 must be understood as: Yield (kg/ha) = $-5447 + 24.0066 \times \text{APAR}_{\text{R1–R6}} + 0.0538 \times \text{APAR}_{\text{CP}^{\wedge}2} -$ (209 IF "Early Sowing" and "La Niña") $-$ (122 IF "Late Sowing" and "La Niña") $-$ (988 IF "Late Sowing" & "Not La Niña").

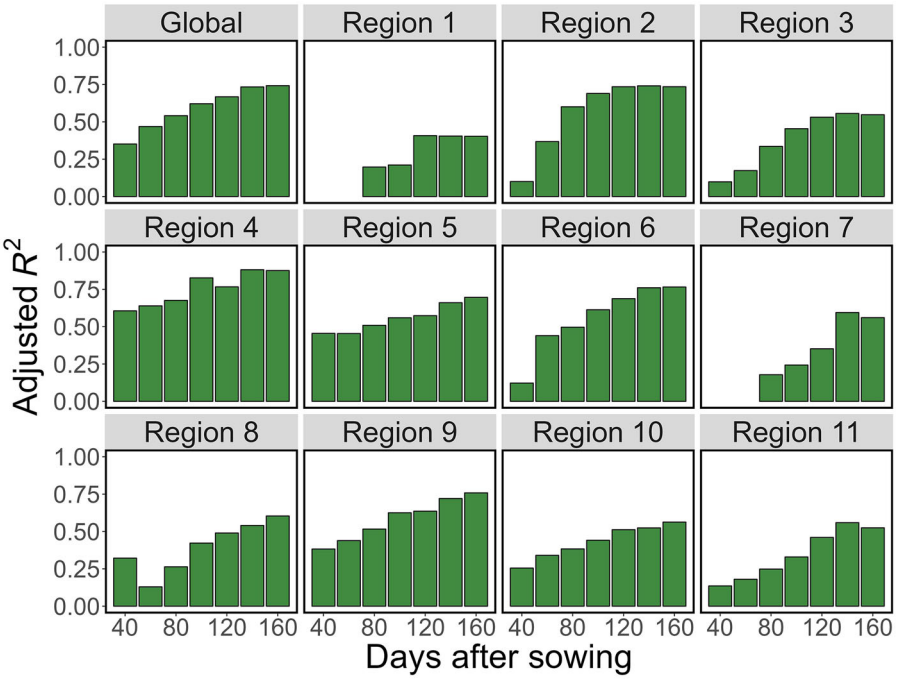

FIGURE 7 R^2_{adj} as a function of days after sowing employed for yield forecast for each region. The top left panel refers to the R^2 of the global database. For the location of the regions, see Figure 1A.

3.3 | Regional-scale yield forecasts throughout the growing season

Model accuracy also increased as the growing season progressed and the predictions were averaged by region instead of individual fields (Figure 10). On the one hand, the progress of the growing season increased accuracy because more fields entered production and more information on APAR was accumulated for each field. On the other hand, as expected, the regional-scale predictions were more accurate than field-scale ones because they averaged out errors (Figures 5–8 vs. Figure 10). For early-sown maize, good accuracy was

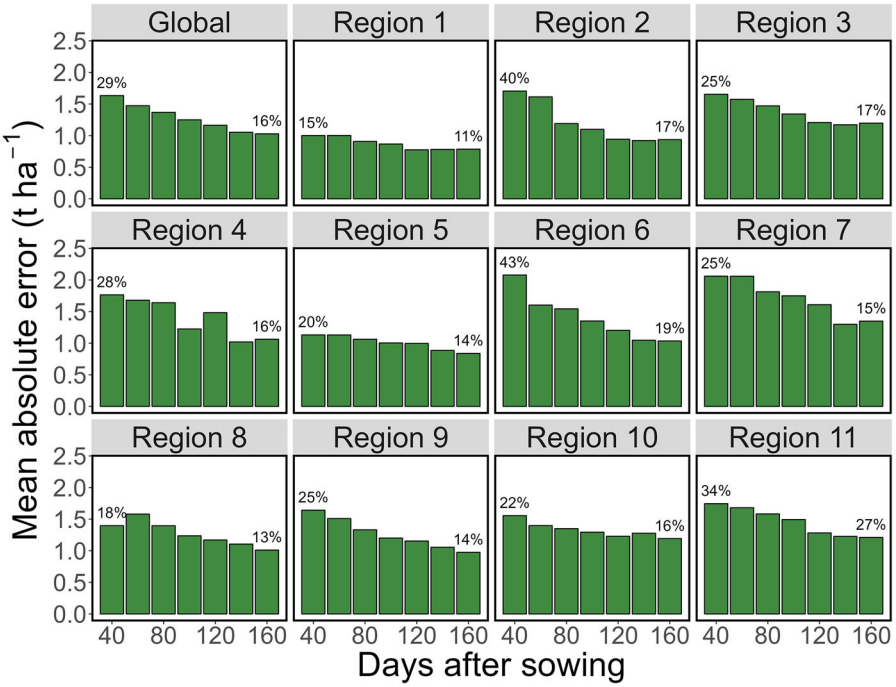

FIGURE 8 Mean absolute error (MAE, t ha^{-1}) as a function of days after sowing employed for yield forecast for each region. The top left panel refers to the mean absolute error (MAE) of the global database. Numbers above the columns refer to the mean absolute percentage error (MAPE, %) for the first and last forecast time during the crop cycle. For the location of the regions, see Figure 1A.

achieved in February, with an MAE of 0.35 t ha^{-1} (MAPE of 4.1%), while for late sowings, it was in May, with an MAE of 0.30 t ha^{-1} (MAPE of 3.8%).

4 | DISCUSSION

Based on satellite information within the framework of Monteith's model, we explained and forecasted maize yield under a wide range of environmental conditions and at different scales. The explanatory and forecasting power of our models ranks within the top tier of the crop yield models reviewed by Schauberger et al. (2020). In addition, our study addressed specific challenges. We worked at the field scale, whereas most other studies forecast at coarser scales, with only a few recent exceptions at the field scale with broad spatio-temporal coverage (Brinkhoff et al., 2024; Deines et al., 2021). Our errors were based on independent validation, whereas half of the revised studies by Schauberger et al. (2020) reported calibration errors. Our models are low-input, as they only require sowing date and a polygon with field boundaries as user inputs. Additionally, they then utilize satellite imagery, temperature, and incident radiation data, all of which are easily obtainable with minimal programming skills (Gorelick et al., 2017). In contrast, many other models rely on extensive environmental and management field data, which are rarely available across fields and years. Finally, our models are easily interpretable in terms of eco-physiological and agronomic factors, whereas others rely on vegetation indices or "black-box" approaches. Therefore, our models serve as a diagnostic tool that allows for the partitioning of yield variation into components such as radiation absorption during different periods within the crop cycle and its conversion efficiency to yield, which encompasses the variation in RUE and HI.

Forecasting field-scale yield at R6 was a matter of partitioning absorbed radiation (APAR) by phenology, inferred from temperature, and differentiating production regions. The APAR up to R6 accounted for only 47% of yield variation. However, APAR by phenological phases accounted for 63% of the variation because the model assigned a higher weight to the reproductive phase, which likely captures a fraction of the variation in HI, as the numerical components of yield, such as grain number and weight, are determined during this phase (Cerrudo et al., 2013; Maddonni et al., 1998; Otegui & Bonhomme, 1998). Additionally, specific APAR-based models for each region accounted for 74% of the overall yield variation. These regions have contrasting soil, climate, and crop management characteristics, thus capturing part of the variation in RUE and HI (Andrade et al., 1992, 1993; Echarte & Andrade, 2003). A key strength of APAR-based models is their ability to capture the effects of environmental stresses, such as water and nutrient limitations, through the radiation absorption component (fAPAR). In summary, based on this work, any stakeholder can forecast field-level maize yield at the R6 stage in Argentina with an average error of 1 t ha^{-1}. In Argentina, the R6 stage usually occurs 30 days before

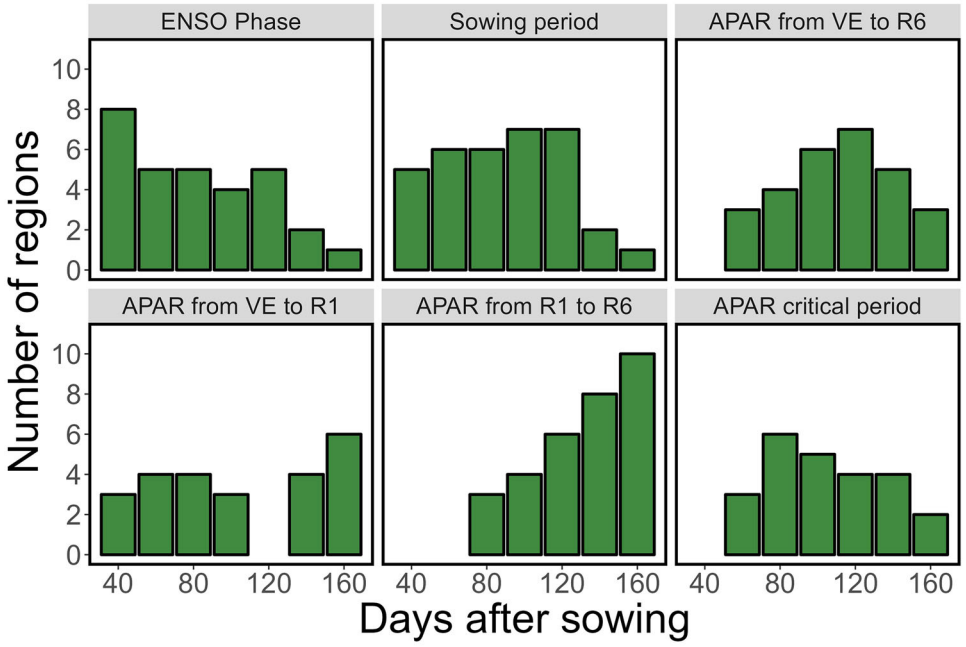

FIGURE 9 Number of regions that incorporated each variable into the models as the days after sowing advanced. Absorbed photosynthetically active radiation (APAR): absorbed radiation (MJ m^{-2}). VE to R6: emergence to physiological maturity. VE to R1: emergence to silking. R1 to R6: silking to physiological maturity. Critical period: 220˚C the day before silking (R1) and 200˚C the day after. ENSO, El Niño-Southern Oscillation.

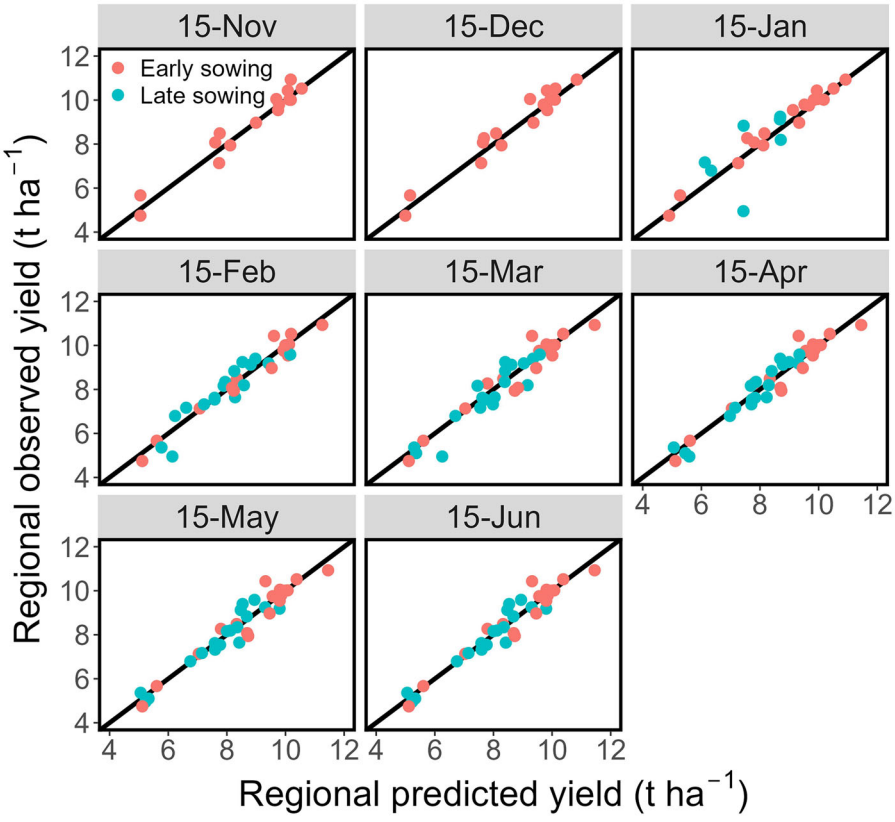

FIGURE 10 Regional observed yield as a function of regional predicted yield. Each panel represents a different calendar date of the growing season. Each point represents a unique combination of region, year, and sowing period. A total of 35 unique combinations were used, 17 corresponding to early sowings (red dots) and 18 to late sowings (blue dots).

harvest for early sowings and up to 90 days for late sowings. To obtain this forecast, our models only require the sowing date and the location of the field, which opens possibilities for the development of computer applications to meet this demand.

Forecasting yield at the field scale earlier than R6 is also valuable and challenging. Our results suggest that any analysts attempting to forecast yield at the field scale may start with a set of baseline data and then may incorporate information about APAR and its impact on yield. The variables that best forecast field-level yield early on are the region where the field is located, the sowing period, and the forecast of the ENSO phase. Thus, the best forecast at the field scale at that time is simply the region yield average under the analyzed context (potentially weighted by knowledge of the specific field's yield potential). Naturally, in some regions of Argentina, either the ENSO phase does not have a marked effect, or the sowing date is exclusively early or late (Otegui et al., 2021). In these cases, these variables lack explanatory power. As the crop cycle progresses, differences in APAR among fields become apparent, and the accuracy of the forecasts increases. Further into the crop cycle, APAR can be differentiated by phenological phase and consequently improve forecasts. Thus, APAR during the reproductive phase becomes more important. APAR during the CP is only significant around crop flowering when grain number is defined (80–120 days after sowing; Cerrudo et al., 2013). Afterward, APAR during the reproductive phase replaces this variable as it integrates and adds information about the other numerical component of yield: grain weight. This finding is supported by the large effect of crop growth during the grain-filling period on final maize kernel weight (Borrás et al., 2004). These responses turn the kernel weight determination period as important as the kernel set CP in many field conditions (Otegui et al., 2021). The prevailing role of APAR in explaining yield should not be interpreted as a lack of effect of sowing period or ENSO phase on yield. Rather, APAR captures those effects and more.

Analysts attempting to forecast maize yield in Argentina at a regional scale throughout the growing season face a dynamic scenario of fields entering production at different times in different regions and two contrasting production systems: early and late sowings. According to the results of this study, they can rely on a library of models that will provide the best forecast for each field at each time point. Additionally, by averaging the forecasts at the regional scale, they can forecast yield with higher accuracy than at the field scale. This gain in accuracy at a coarser level is in part due to the cancellation of errors when aggregating predictions and the lower variability at this scale (Deines et al., 2021). In Argentina, forecasts at the regional scale need to be differentiated according to the early and late sowing systems. In this study, the errors did not differ between them, demonstrating that the developed models are applicable even in contrasting production systems. Simply put, the two systems are incorporated into the growing season at different periods. Therefore, the best forecast is achieved in February for early sowings (30 days before harvest) and in May for late sowings (up to 90 days before harvest). When combined with an estimation of the harvested area, the harvest volume can be estimated with a known error.

We speculate here on the sources of the variation not accounted for by our models. Likely, some are errors in estimating yield and APAR. Yield in our dataset was estimated at the farm level, based on the grain leaving the field and an estimation of harvested area, both subject to error. The sources of error behind our estimate of APAR are complex. Field boundaries were not perfectly delimited, pixels did not cover the entire surface, and NDVI was transformed into fAPAR through calibration models, which may be particularly uncertain at early growth stages due to low canopy cover and soil or residue background effects (Gitelson et al., 2014). In addition, using monthly PARinc and 16-day NDVI may smooth short-term variability and increase APAR uncertainty during rapid canopy growth. More interestingly, however, what our models did not capture of yield variations speaks of the variation of RUE and HI; in other words, the true variation of the grain conversion efficiency from radiation to yield. RUE is affected by above-optimum (Rattalino Edreira & Otegui, 2012) and suboptimum (Andrade et al., 1993) temperatures, which may modify conversion efficiency differently across regions, sowing dates, and growth stages. Similarly, the HI is defined all along the grain-filling period (Muchow et al., 1990), being very stable in most growth conditions but particularly sensitive to stress during the CP (Sinclair et al., 1990). In addition, RUE and HI may interact with APAR (Earl & Davis, 2003), which determines that they are not merely the residuals of the model based on APAR. By discriminating APAR by phenology, our models probably accounted for a great proportion of the variation of RUE, HI, and this interaction. Yet, on average, up to 1 t ha^{-1} of yield variation (16%) may be attributed to unaccounted variation of conversion efficiency, including grain lost before harvest. In fact, grain conversion efficiency varied more than APAR across the dataset (Table 2). Understanding this variation can provide information about specific maize genotypes or environments that convert APAR into yield more or less efficiently—for example, by comparing fields with and without stress conditions such as drought or nutrient limitations (Andrade et al., 1993; Chazarreta et al., 2024; Kiniry, 1990; Neiff et al., 2016). This type of conversion efficiency analysis may guide management practices toward maximizing this component and ultimately enhancing crop yield.

A robust yield estimation system could benefit the agricultural sector by forecasting and explaining yield variations at different scales. In terms of forecasting at the field and farm scales, yield forecasts allow farmers to evaluate the

progress of their crops in real-time and make decisions that improve their harvest and storage logistics. Agricultural credit and insurance companies would also improve their payment systems and reduce their operating costs at the field level. At larger scales, regional yield forecasts allow governments and NGOs to design policies and mobilize resources more efficiently in critical situations (e.g., drought). Grain supply chain agents, such as collectors or exporting companies, would also benefit from such regional forecasts. Collectively, all these benefits may have larger impacts on final economic revenue than environmental limitations to crop growth (Rattalino Edreira et al., 2018). In terms of explaining yield, such a system would allow producers and technicians to analyze the past agricultural seasons with information on the radiation absorbed by the crop. In this way, yield variation could be decomposed into variation in radiation absorption (PARinc and fAPAR) and conversion efficiency to yield (RUE and HI). Additionally, the system would allow us to detect fields whose expected yield varied throughout the season. For example, fields that started with "high" yield estimates and ended with "low" estimates, or vice versa, may inform on the environmental controls that determined final yield. In summary, having a crop yield estimation system during the cycle would significantly benefit a large part of the agricultural sector at a range of scales.

5 | CONCLUSION

In this study, we developed models that forecast maize yield at the field and regional scales, using only the sowing date and field location as inputs requested from the users. These models were based on the crop's absorbed radiation estimated from satellites and easily obtainable information such as the ENSO phase or the sowing period. The forecasts at physiological maturity, 30–90 days before harvest, had an average error of 1 t ha^{-1} at the field scale and 0.3 t ha^{-1} at the regional scale. As the forecast was attempted earlier than the physiological maturity, the error gradually increased due to the loss of information on absorbed radiation. In addition to providing a yield forecast, the models can be used to understand the environmental controls that defined yield in the past. Thus, the results of this study allow different stakeholders in the maize supply chain to obtain accurate information for decision-making based on objective yield data from one of the world's most important areas in terms of maize production and export.

AUTHOR CONTRIBUTIONS

Martin Menendez-Coccoz: Conceptualization; formal analysis; investigation; methodology; writing—original draft. **Diego H. Rotili**: Conceptualization; methodology; writing—review and editing. **Maria E. Otegui**: Conceptualization; methodology; writing—review and editing. **Gustavo Martini**: Data curation; writing—review and editing. **Maria Paolini**: Data curation; writing—review and editing. **Carlos Di Bella**: Writing—review and editing. **Gervasio Piñeiro**: Writing—review and editing. **Martín Oesterheld**: Conceptualization; methodology; supervision; writing—review and editing.

ACKNOWLEDGMENTS

We thank all members of the Asociación Argentina de Consorcios Regionales de Experimentación Agrícola (AACREA) for sharing their production data. Part of the satellite data processing was performed by the Laboratorio de Análisis Regional y Teledetección (LART). MMC was partially supported by a "UBA200" scholarship from Universidad de Buenos Aires. DHR held a postdoctoral fellowship from CONICET. This study was funded by grants from FONCyT (PICT2016-1258, PICT2020-02102) and UBACyT.

CONFLICT OF INTEREST STATEMENT

The authors declare no conflicts of interest.

DATA AVAILABILITY STATEMENT

Except for latitude–longitude of each field year, all data will be available on request.

ORCID

Martin Menendez-Coccoz https://orcid.org/0009-0005-9705-7381

REFERENCES

Andrade, F. H., Uhart, S. A., Arguissain, G. G., & Ruiz, R. A. (1992). Radiation use efficiency of maize grown in a cool area. *Field Crops Research*, *28*(4), 345–354. https://doi.org/10.1016/0378-4290(92)90020-A

Andrade, F. H., Uhart, S. A., & Cirilo, A. (1993). Temperature affects radiation use efficiency in maize. *Field Crops Research*, *32*(1–2), 17–25. https://doi.org/10.1016/0378-4290(93)90018-I

Andrade, J. F., Ermacora, M., & Satorre, E. H. (2022). Assessing benefits of land use intensification on extensive grain cropping systems of the Pampas. *European Journal of Agronomy*, *135*, 126484. https://doi.org/10.1016/j.eja.2022.126484

Basso, B., & Liu, L. (2019). Seasonal crop yield forecast: Methods, applications, and accuracies. In D. L. Sparks (Eds.), *Advances in agronomy* (Vol. 154, pp. 201–255), Academic Press Inc. https://doi.org/10.1016/bs.agron.2018.11.002

Benami, E., Jin, Z., Carter, M. R., Ghosh, A., Hijmans, R. J., Hobbs, A., Kenduiywo, B., & Lobell, D. B. (2021). Uniting remote sensing, crop modelling and economics for agricultural risk management. *Nature Reviews Earth & Environment*, *2*, 140–159. https://doi.org/10.1038/s43017-020-00122-y

Borrás, L., Slafer, G. A., & Otegui, M. E. (2004). Seed dry weight response to source–sink manipulations in wheat, maize and soybean: A quantitative reappraisal. *Field Crops Research*, *86*(2–3), 131–146. https://doi.org/10.1016/j.fcr.2003.08.002

Brinkhoff, J., Clarke, A., Dunn, B. W., & Groat, M. (2024). Analysis and forecasting of Australian rice yield using phenology-based aggregation of satellite and weather data. *Agricultural and Forest Meteorology*, *353*, 110055. https://doi.org/10.1016/j.agrformet.2024.110055

Burke, M., Driscoll, A., Lobell, D. B., & Ermon, S. (2020). Using satellite imagery to understand and promote sustainable development. *Science*, *371*, eabe8628. https://doi.org/10.1126/science.abe8628

Cerrudo, A., Di Matteo, J., Fernandez, E., Robles, M., Olmedo Pico, L., & Andrade, F. H. (2013). Yield components of maize as affected by short shading periods and thinning. *Crop and Pasture Science*, *64*, 580–587. https://doi.org/10.1071/CP13201

Chazarreta, Y. D., Álvarez Prado, S., Giménez, V. D., Carcedo, A. J. P., López, C. G., Ciampitti, I. A., & Otegui, M. E. (2024). Yield determination of temperate maize hybrids with different end-uses: An ecophysiological analysis. *Crop Science*, *65*, e21414. https://doi.org/10.1002/csc2.21414

Chipanshi, A. C., Ripley, E. A., & Lawford, R. G. (1997). Early prediction of spring wheat yields in Saskatchewan from current and historical weather data using the CERES-Wheat model. *Agricultural and Forest Meteorology*, *84*(3–4), 223–232. https://doi.org/10.1016/S0168-1923(96)02363-5

Cirilo, A. G., & Andrade, F. H. (1994). Sowing date and maize productivity: I. Crop growth and dry matter partitioning. *Crop Science*, *34*(4), 1039–1043. https://doi.org/10.2135/cropsci1994.0011183X003400040037x

Deines, J. M., Patel, R., Liang, S. Z., Dado, W., & Lobell, D. B. (2021). A million kernels of truth: Insights into scalable satellite maize yield mapping and yield gap analysis from an extensive ground dataset in the US Corn Belt. *Remote Sensing of Environment*, *253*, 112174. https://doi.org/10.1016/j.rse.2020.112174

Didan, K., Munoz, A. B., Solano, R., & Huete, A. (2015). *MODIS vegetation index user's guide (MOD13 series)*. University of Arizona: Vegetation Index and Phenology Lab.

Earl, H. J., & Davis, R. F. (2003). Effect of drought stress on leaf and whole canopy radiation use efficiency and yield of maize. *Agronomy Journal*, *95*(3), 688–696. https://doi.org/10.2134/agronj2003.6880

Echarte, L., & Andrade, F. H. (2003). Harvest index stability of Argentinean maize hybrids released between 1965 and 1993. *Field Crops Research*, *82*(1), 1–12. https://doi.org/10.1016/S0378-4290(02)00232-0

FAO. (2023). *FAOSTAT: Crops and livestock products*. https://www.fao.org/faostat/en/#data/QCLc

Fritz, S., See, L., Bayas, J. C. L., Waldner, F., Jacques, D., Becker-Reshef, I., Whitcraft, A., Baruth, B., Bonifacio, R., Crutchfield, J., Rembold, F., Rojas, O., Schucknecht, A., Van der Velde, M., Verdin, J., Wu, B., Yan, N., You, L., Gilliams, S., … McCallum, I. (2019). A comparison of global agricultural monitoring systems and current gaps. *Agricultural Systems*, *168*, 258–272. https://doi.org/10.1016/j.agsy.2018.05.010

Gitelson, A. A., Peng, Y., & Huemmrich, K. F. (2014). Relationship between fraction of radiation absorbed by photosynthesizing maize and soybean canopies and NDVI from remotely sensed data taken at close range and from MODIS 250m resolution data. *Remote Sensing of Environment*, *147*, 108–120. https://doi.org/10.1016/j.rse.2014.02.014

Gorelick, N., Hancher, M., Dixon, M., Ilyushchenko, S., Thau, D., & Moore, R. (2017). Google earth engine: Planetary-scale geospatial analysis for everyone. *Remote Sensing of Environment*, *202*, 18–27. https://doi.org/10.1016/j.rse.2017.06.031

Hodges, T., Botner, D., Sakamoto, C., & Haug, J. H. (1987). Using the CERES-maize model to estimate production for the US Cornbelt. *Agricultural and Forest Meteorology*, *40*(4), 293–303. https://doi.org/10.1016/0168-1923(87)90043-8

Huang, J., Gómez-Dans, J. L., Huang, H., Ma, H., Wu, Q., Lewis, P. E., Liang, S., Chen, Z., Xue, J. H., Wu, Y., Zhao, F., Wang, J., & Xie, X. (2019). Assimilation of remote sensing into crop growth models: Current status and perspectives. *Agricultural and Forest Meteorology*, *276–277*, 107609. https://doi.org/10.1016/j.agrformet.2019.06.008

Irisarri, G., Oyarzabal, M., Arocena, D., Vassallo, M., & Oesterheld, M. (2018). *Focus: Software de gestión de información satelital para observar recursos naturales (versión 2018)*. LART, IFEVA, Universidad de Buenos Aires, CONICET, Buenos Aires, Argentina. http://focus.agro.uba.ar

Johnson, D. M. (2014). An assessment of pre- and within-season remotely sensed variables for forecasting corn and soybean yields in the United States. *Remote Sensing of Environment*, *141*, 116–128. https://doi.org/10.1016/j.rse.2013.10.027

Kiniry, J. R. (1990). Variability in radiation-use efficiency associated with vapor-pressure deficit. *Field Crops Research*, *25*, 171–181. https://doi.org/10.1016/0378-4290(90)90001-R

Kuhn, M. (2008). Building predictive models in R using the caret package. *Journal of Statistical Software*, *28*, 1–26. https://doi.org/10.18637/jss.v028.i05

Lindquist, J. L., Arkebauer, T. J., Walters, D. T., Cassman, K. G., & Dobermann, A. (2005). Maize radiation use efficiency under optimal growth conditions. *Agronomy Journal*, *97*(1), 72–78. https://doi.org/10.2134/agronj2005.0072

Lobell, D. B. (2013). The use of satellite data for crop yield gap analysis. *Field Crops Research*, *143*, 56–64. https://doi.org/10.1016/j.fcr.2012.08.008

Maddonni, G. A. (2012). Analysis of the climatic constraints to maize production in the current agricultural region of Argentina-a probabilistic approach. *Theoretical and Applied Climatology*, *107*(3–4), 325–345. https://doi.org/10.1007/s00704-011-0478-9

Maddonni, G. A., Otegui, M. E., & Bonhomme, R. (1998). Grain yield components in maize: II. Postsilking growth and kernel weight. *Field Crops Research*, *56*(3), 257–264. https://doi.org/10.1016/S0378-4290(97)00094-4

Martins, F. R., Pereira, E. B., Gonçalves, A. R., Costa, R. S., Lima, F. J. L. D., Rüther, R., Abreu, S., Tiepolo, G. M., Pereira, S. V., & Souza, J. G. D. (2017). *Atlas brasileiro de energia solar* (2nd ed.). INPE. https://doi.org/10.34024/978851700089

Mercau, J. L., & Otegui, M. E. (2014). A modeling approach to explore water management strategies for late-sown maize and double-cropped wheat–maize in the rainfed Pampas region of Argentina. In L. R. Ahuja, L. Ma, & R. J. Lascano (Eds.), *Practical applications of agricultural system models to optimize the use of limited water* (pp. 351–373). ASA, CSSA, SSSA.

Monteith, J. L. (1972). Solar radiation and productivity in tropical ecosystems. *Journal of Applied Ecology*, *9*(3), 747–766. https://doi.org/10.2307/2401901

Monteith, J. L. (1994). Principles of resource capture by crop stands. In J. L. Monteith, R. K. Scott, & M. H. Unsworth (Eds.), *Resource capture by crops* (pp. 1–15). Nottingham University Press.

Muchow, R. C., Sinclair, T. R., & Bennett, J. M. (1990). Temperature and solar radiation effects on potential maize yield across locations. *Agronomy Journal*, *82*(2), 338–343. https://doi.org/10.2134/agronj1990.00021962008200020033x

Murata, Y. (1975). Estimation and simulation of rice yield from climatic factors. *Agricultural Meteorology*, *15*(1), 117–131. https://doi.org/10.1016/0002-1571(75)90023-0

Neiff, N., Trachsel, S., Valentinuz, O. R., Balbi, C. N., & Andrade, F. H. (2016). High temperatures around flowering in maize: Effects on photosynthesis and grain yield in three genotypes. *Crop Science*, *56*(5), 2702–2712. https://doi.org/10.2135/cropsci2015.12.0755

Otegui, M. E., Andrade, F. H., Cirilo, A., & Mercau, J. (2023). Fecha de siembra. In F. Andrade, M. E. Otegui, A. Cirilo, & S. Uhart (Eds.), *Ecofisiología y manejo del cultivo de maíz* (pp. 311–327). Editorial Maizar. https://sites.google.com/agro.uba.ar/libroecofisiologadelcultivodem/inicio

Otegui, M. E., & Bonhomme, R. (1998). Grain yield components in maize: I. Ear growth and kernel set. *Field Crops Research*, *56*(3), 247–256. https://doi.org/10.1016/S0378-4290(97)00093-2

Otegui, M. E., Nicolini, M. G., Ruiz, R. A., & Dodds, P. A. (1995). Sowing date effects on grain yield components for different maize genotypes. *Agronomy Journal*, *87*(1), 29–33. https://doi.org/10.2134/agronj1995.00021962008700010006x

Otegui, M. E., Riglos, M., & Mercau, J. L. (2021). Genetically modified maize hybrids and delayed sowing reduced drought effects across a rainfall gradient in temperate Argentina. *Journal of Experimental Botany*, *72*(14), 5180–5188. https://doi.org/10.1093/jxb/erab139

Paudel, D., Boogaard, H., de Wit, A., van der Velde, M., Claverie, M., Nisini, L., Janssen, S., Osinga, S., & Athanasiadis, I. N. (2022). Machine learning for regional crop yield forecasting in Europe. *Field Crops Research*, *276*, 108377. https://doi.org/10.1016/j.fcr.2021.108377

Pellegrini, P., Cossani, C. M., Bella, C. D., Piñeiro, G., Sadras, V. O., & Oesterheld, M. (2020). Simple regression models to estimate light interception in wheat crops with Sentinel-2 and a handheld sensor. *Crop Science*, *60*(3), 1607–1616. https://doi.org/10.1002/csc2.20129

Peralta, N. R., Assefa, Y., Du, J., Barden, C. J., & Ciampitti, I. A. (2016). Mid-season high-resolution satellite imagery for forecasting site-specific corn yield. *Remote Sensing*, *8*, 848. https://doi.org/10.3390/rs8100848

Podestá, G. P., Messina, C. D., Grondona, M. O., & Magrin, G. O. (1999). Associations between grain crop yields in central-eastern Argentina and El Niño–Southern Oscillation. *Journal of Applied Meteorology Climatology*, *38*, 1488–1498. https://doi.org/10.1175/1520-0450(1999)038⟨1488:ABGCYI⟩2.0.CO;2

QGIS Development Team. (2022). *QGIS Geographic information system*. Open Source Geospatial Foundation Project. http://qgis.osgeo.org

R Core Team. (2021). *R: A language and environment for statistical computing*. R Foundation for Statistical Computing. https://www.R-project.org/

Rattalino Edreira, J. I., Guilpart, N., Sadras, V., Cassman, K. G., van Ittersum, M. K., Schils, R. L., & Grassini, P. (2018). Water productivity of rainfed maize and wheat: A local to global perspective. *Agricultural and Forest Meteorology*, *259*, 364–373. https://doi.org/10.1016/j.agrformet.2018.05.019

Rattalino Edreira, J. I., Mourtzinis, S., Azzari, G., Andrade, J. F., Conley, S. P., Lobell, D., Specht, J. E., & Grassini, P. (2020). From sunlight to seed: Assessing limits to solar radiation capture and conversion in agro-ecosystems. *Agricultural and Forest Meteorology*, *280*, 107775. https://doi.org/10.1016/j.agrformet.2019.107775

Rattalino Edreira, J. I., & Otegui, M. E. (2012). Heat stress in temperate and tropical maize hybrids: Differences in crop growth, biomass partitioning and reserves use. *Field Crops Research*, *130*, 87–98. https://doi.org/10.1016/j.fcr.2012.02.009

ReTAA. (2022). *Relevamiento de tecnología agrícola aplicada*. Ministerio de Agricultura, Ganadería y Pesca. https://www.bolsadecereales.com/tecnologia-informes

Ritchie, S. W., & Hanway, J. J. (1982). *How a corn plant develops* (Special report No. 48). Iowa State University.

Satorre, E. H., & Andrade, J. F. (2022). El maíz en los sistemas productivos de Argentina: Un análisis global y regional de su desarrollo reciente. In F. H. Andrade, M. E. Otegui, A. Cirilo, & S. Uhart (Eds.), *Ecofisiología y manejo del cultivo de maíz* (pp. 25–50). INTA.

Schauberger, B., Jägermeyr, J., & Gornott, C. (2020). A systematic review of local to regional yield forecasting approaches and frequently used data resources. *European Journal of Agronomy*, *120*, 126153. https://doi.org/10.1016/j.eja.2020.126153

Schwalbert, R. A., Amado, T. J. C., Nieto, L., Varela, S., Corassa, G. M., Horbe, T. A. N., Rice, C. W., Peralta, N. R., & Ciampitti, I. A. (2018). Forecasting maize yield at field scale based on high-resolution satellite imagery. *Biosystems Engineering*, *171*, 179–192. https://doi.org/10.1016/j.biosystemseng.2018.04.020

Sinclair, T. R., Bennett, J. M., & Muchow, R. C. (1990). Relative sensitivity of grain yield and biomass accumulation to drought in field-grown maize. *Crop Science*, *30*(3), 690–693. https://doi.org/10.2135/cropsci1990.0011183X003000030043x

Thompson, L. M. (1969). *Weather and Technology in the Production of Corn in the U. S. Corn Belt*. https://doi.org/10.2134/agronj1969.00021962006100030037x

van der Velde, M., Biavetti, I., El-Aydam, M., Niemeyer, S., Santini, F., & van den Berg, M. (2019). Use and relevance of European Union crop monitoring and yield forecasts. *Agricultural Systems*, *168*, 224–230. https://doi.org/10.1016/j.agsy.2018.05.001

Wickham, H., Averick, M., Bryan, J., Chang, W., McGowan, L., François, R., Grolemund, G., Hayes, A., Henry, L., Hester, J., Kuhn, M., Pedersen, T., Miller, E., Bache, S., Müller, K., Ooms, J., Robinson, D., Seidel, D., Spinu, V., & Yutani, H. (2019). Welcome to the tidyverse. *Journal of Open Source Software*, *4*(43), 1686. https://doi.org/10.21105/joss.01686)

SUPPORTING INFORMATION

Additional supporting information can be found online in the Supporting Information section at the end of this article.

How to cite this article: Menendez-Coccoz, M., Rotili, D. H., Otegui, M. E., Martini, G., Paolini, M., Di Bella, C., Piñeiro, G., & Oesterheld, M. (2025). Low-input, interpretable models to forecast maize yield at multiple scales based on absorbed radiation. *Agronomy Journal*, *117*, e70089. https://doi.org/10.1002/agj2.70089